Published in final edited form as:

Biochemistry. 2006 January 10; 45(1): 167–174. doi:10.1021/bi051729t.

A New Approach to Producing Functional Gα Subunits Yields the Activated and Deactivated Structures of $G\alpha_{12/13}$ Proteins [†]

Barry Kreutz[‡], **Douglas M. Yau**[‡], **Mark Nance**[§], **Shihori Tanabe**[‡], **John J. G. Tesmer**[§,*], and **Tohru Kozasa**[‡,*]

Department of Pharmacology, Life Sciences Institute, The University of Michigan, 210 Washtenaw Ave, Ann Arbor, Michigan 48109-2216

Summary

The oncogenic $G_{12/13}$ subfamily of heterotrimeric G proteins transduces extracellular signals that regulate the actin cytoskeleton, cell cycle progression, and gene transcription. Previously, structural analyses of fully-functional $G\alpha_{12/13}$ subunits have been hindered by insufficient amounts of homogeneous, functional protein. Herein we report that substitution of the N-terminal helix of $G\alpha_{i1}$ for the corresponding region of $G\alpha_{12}$ or $G\alpha_{13}$ generated soluble chimeric subunits ($G\alpha_{i/12}$ and $G\alpha_{i/13}$) that could be purified in sufficient amounts for crystallographic studies. Each chimera bound guanine nucleotides, Gβγ subunits and effector proteins, and exhibited GAP responses to p115RhoGEF and leukemia-associated RhoGEF. Like their wild-type counterparts, $G\alpha_{i/13}$, but not $G\alpha_{i/12}$, stimulated the activity of p115RhoGEF. Crystal structures of the $G\alpha_{i/12}$·GDP·AlF_4^- and $G\alpha_{i/13}$·GDP complexes were determined using diffraction data extending to 2.9 and 2.0 Å, respectively. These structures reveal not only the native structural features of $G\alpha_{12}$ and $G\alpha_{13}$ subunits, which are expected to be important for their interactions with GPCRs and effectors such as Gα-regulated RhoGEFs, but also novel conformational changes that are likely coupled to GTP hydrolysis in the $G\alpha_{12/13}$ class of heterotrimeric G proteins.

Heterotrimeric GTP-binding proteins (G proteins) receive inputs from G protein-coupled receptors (GPCRs) at the cell surface and elicit a wide variety of responses within the cell (1). Activation of GPCRs by extracellular stimuli induces the Gα subunit to release its bound GDP and bind GTP, and facilitates dissociation of Gα·GTP from the β and γ subunits (Gβγ). Both Gα·GTP and Gβγ subsequently bind to and regulate the activity of various effector molecules. A family known as regulator of G protein signaling (RGS) proteins can bind to activated Gα subunits and accelerate their rate of deactivation, thereby serving as GTPase-activating proteins (GAPs) (2). It was shown through biochemical and structural studies of RGS4 that its core helical domain, referred to herein as the RGS homology (RH) domain[1], binds to all three switch regions of Gα and thereby stabilizes the transition state for GTP hydrolysis (3,4).

[†]Support was provided by National Institute of Health Grant HL071818, American Heart Association Scientist Development Grant 0235273N and an American Cancer Society Research Scholar grant (to JJGT), National Institutes of Health Grants GM61454 and NS41441 and an American Heart Established Investigator Award 0040006N (to TK) and a Predoctoral fellowship from the American Heart Association Midwest Affiliate 0315253Z (to BK).

*To whom correspondence should be addressed. E-mail: E-mail: johntesmer@umich.edu. Telephone: (734) 615-9544. Fax: (734) 763-6492. E-mail: tkozas@uic.edu. Telephone: (312)-413-0111. FAX: (312)-996-1225.

[‡]Department of Pharmacology, University of Illinois & College of Medicine, Chicago, IL 60612

[§]Institute for Cell and Molecular Biology, Department of Chemistry and Biochemistry, University of Texas, Austin, TX 78712; Department of Pharmacology, Life Sciences Institute, University of Michigan, Ann Arbor MI 48109.

[1]We refer to the core domain of RGS4 as an RGS homology (RH) domain in order to distinguish between the fold of this domain and its function. For example, while RGS proteins serve as Gα GAPs, domains in G protein-coupled receptor kinases and axin that are homologous to those found in RGS proteins (RH domains) have distinct functions.

Among the four subfamilies of Gα subunits (5), the members of the $G\alpha_{12/13}$ subfamily are distinct in that they are potently oncogenic in cell-based assays (6,7). Stimulation of $G\alpha_{12/13}$-coupled receptors, such as those for thrombin or lysophosphatidic acid, transforms cells in a manner implicating the activation of Rho family GTPases (8,9). Downstream effector targets of $G\alpha_{12/13}$ subunits are diverse and include cadherin (10), protein phosphatase 5 (11) and many others (12). However, the best-characterized targets of $G\alpha_{12/13}$ subunits are a family of Rho guanine nucleotide exchange factors (RhoGEFs), including p115RhoGEF, leukemia-associated RhoGEF (LARG), and PDZ-RhoGEF (13–15). Each of these RhoGEFs contains an RH domain (also known as the rgRGS or LH domain)[1] that binds specifically to activated $G\alpha_{12/13}$ subunits (16). Unlike RGS proteins, the RhoGEF RH domain binds to the effector-binding site of the Gα subunit rather than the site traditionally used by RGS proteins (17). A small, acidic domain N-terminal to the RH domain, which is essential for GAP activity but not for the binding of $G\alpha_{13}$ (18,19), occupies the binding site traditionally used by RGS proteins.

Biochemical and crystallographic characterization of $G\alpha_{12/13}$ subunits and their effector complexes requires large amounts of homogeneous, fully-functional $G\alpha_{12}$ and $G\alpha_{13}$ subunits, which previously have been produced with exceptionally low yields (20,21). Although Chen *et al.* were able to express a "$G\alpha_{13/i}$-5" chimera, in which the switch regions and α-helical domain of $G\alpha_{13}$ were swapped for those of $G\alpha_{i1}$, the resulting chimera exhibited approximately a 10-fold higher nucleotide exchange rate and 5% of the GAP activity of wild-type $G\alpha_{13}$ in response to p115RhoGEF. Even so, it could still be crystallized as a complex with an N-terminal fragment of p115RhoGEF that included its RH domain (17).

Herein we show that substitution of the N-terminal helix of $G\alpha_{i1}$ for the corresponding region of $G\alpha_{12}$ and $G\alpha_{13}$ generated soluble $G\alpha_{i/12}$ and $G\alpha_{i/13}$ chimera that retained all wild-type biochemical properties while also being expressed at much greater levels than their wild-type counterparts. By determining the crystal structures of the $G\alpha_{i/12}\cdot GDP\cdot AlF_4^-$ (activated) and $G\alpha_{i/13}\cdot GDP$ (deactivated) complexes, we not only show that these proteins are suitable for structural studies, but also provide the first look at the native atomic structures of these oncogenic G protein subunits and a novel conformational change upon deactivation of these subunits that we propose is specific to the $G\alpha_{12/13}$ subfamily. Differences in the structures of $G\alpha_{12}$ and $G\alpha_{13}$ undoubtedly contribute to their differential ability to couple with receptors and to regulate downstream effectors.

Experimental Procedures

Expression constructs

The $G\alpha_{i/13}$ chimera was created by ligating the N-terminal coding region of rat $G\alpha_{i1}$ (residues 1–28) to $G\alpha_{13}$ (residues 47–377) and subcloning the product into the baculovirus transfer vector pFastBacHT$_A$ (Invitrogen, Carlsbad, CA). A construct of $G\alpha_{i/12}$ was created using the same strategy. Each construct therefore includes an N-terminal hexahistidine (His_6) tag followed by a tobacco etch virus (TEV) protease recognition site. The expression construct for glutathione-*S*-transferase (GST)-p115-RH or GST-LARG-RH was generated by subcloning the coding region of p115RhoGEF (residues 1 to 252) or LARG (residues 319 to 598) into pGEX-KG, respectively.

Production of chimeric Gα subunits

All purification steps were conducted at 4°C using ice-cold buffers supplemented with protease inhibitors. Cells from 4 liters of Sf9 culture were harvested 48 h after infection with 15 ml/L of either $G\alpha_{i/13}$ or $G\alpha_{i/12}$ amplified baculovirus stock, resuspended in 400 ml of Lysis Buffer (20 mM HEPES pH 8.0, 0.1 mM EDTA, 10 mM 2-mercaptoethanol (βME), 1 mM $MgCl_2$, 100 mM NaCl, and 10 μM GDP), and then lysed by nitrogen cavitation. Lysates were centrifuged at 100,000 × *g* for 30 min, after which the supernatants were diluted with 1600 ml of Buffer A (20 mM HEPES pH 8.0, 10 mM βME, 1 mM $MgCl_2$, 100 mM NaCl, 10 μM GDP, and 12.5 mM imidazole, pH 8.0) and loaded onto a Ni-NTA agarose (Qiagen, Valencia, CA) column equilibrated with Buffer A. The column was washed with 20 volumes of Buffer B (Buffer A containing 0.4 M NaCl and 20 mM imidazole, pH 8.0), and the chimera was eluted in 10 fractions of 1 volume of Buffer C (Buffer A containing 150 mM imidazole, pH 8.0). Peak fractions were supplemented with 10% glycerol, and exchanged to Buffer D (20 mM HEPES pH 8.0, 10 mM βME, 1 mM $MgCl_2$, 100 mM NaCl, 10 μM GDP, 10% glycerol) with Centricon Plus-20 PL-30 (Millipore, Billerica, MA).

Purification of RH proteins

GST-p115-RH was produced in JM109 harboring pGEX-KG/p115-RH and pT-Trx plasmids (22) for 3 hr after induction with 0.1 mM IPTG at 30°C. GST-LARG-RH was similarly expressed in BL21(DE3) CodonPlus RP (Stratagene, La Jolla, CA) harboring the pGEX-KG/LARG-RH plasmid. GST-RH fusions were purified by glutathione Sepharose 4B resin (Amersham Biosciences).

Interaction of chimeric Gα subunits with RH proteins

$G\alpha_{i/13}$ or $G\alpha_{i/12}$ (2 μg) was diluted in Buffer E (20 mM Tris-HCl, pH 8.0, 1 mM EDTA, 10 mM βME, 300 mM NaCl, 10 mM $MgCl_2$, 30 μM GDP, 0.1% $C_{12}E_{10}$), either in the absence or presence of AlF_4^- (30 μM $AlCl_3$ and 10 mM NaF), and mixed with 33 μg of GST-p115-RH or 38 μg of GST-LARG-RH in a final volume of 500 μl. After incubation on ice for 20 min, glutathione Sepharose 4B (30 μl resin) was added and samples were incubated with constant mixing for 1 h at 4°C. Beads were pelleted by centrifugation (600 × *g*, 1 min, 4°C) and washed four times with 400 μl of Buffer E (with or without AlF_4^-). Beads were mixed with 20 mM reduced glutathione and SDS-PAGE sample buffer and boiled for 10 min. Immunoblotting was performed with anti-$G\alpha_{13}$ B860 (21) or anti-$G\alpha_{12}$ J168 (20) antibody.

Rho nucleotide exchange assays

His_6-RhoA was expressed in Sf9 cells and purified as described (23). $G\alpha_{13}$, $G\alpha_{i/13}$, or $G\alpha_{i/12}$ (5 pmol) was first incubated in the presence of AMF (60 μM $AlCl_3$, 5 mM $MgCl_2$, and 20 mM NaF) for 15 min on ice, then incubated with His_6-RhoA (25 pmol) and p115RhoGEF (0.25 pmol) in binding buffer (50 mM Tris-HCl, pH 7.5, 1 mM DTT, 0.5 mM EDTA, 50 mM NaCl, 5 mM $MgCl_2$, 0.05% $C_{12}E_{10}$, and 10 μM GTPγS with ~500 cpm/pmol [^{35}S]-GTPγS) in a final reaction volume of 50 μl. Reactions were terminated after incubation for 5 min at 30°C by addition of wash buffer, and GTPγS binding to RhoA was determined by filter binding as described (24).

Crystallization of $G\alpha_{i/12}$·GDP·AlF_4^- and $G\alpha_{i/13}$·GDP

$G\alpha_{i/13}$ or $G\alpha_{i/12}$ was first incubated with 1.5% (w/w) recombinant TEV protease for 2 hr at 25°C to remove the His_6-tag, and then activated by AlF_4^- (20 μM $AlCl_3$ and 10 mM NaF) for 15 min on ice. This mixture was loaded onto tandem Superdex 200 10/30 gel filtration columns (Amersham Biosciences, Piscataway, NJ) equilibrated in gel filtration buffer (20 mM HEPES pH 8.0, 1 mM EDTA, 2 mM DTT, 5 mM $MgCl_2$, 50 mM NaCl, 10 μM GDP, 20 μM $AlCl_3$, and 10 mM NaF). Both $G\alpha_{i/13}$ and $G\alpha_{i/12}$ eluted from the column as apparent monomers. Peak fractions were pooled and concentrated using a Centricon YM-30 (Millipore).

$G\alpha_{i/12}$ was crystallized by mixing 1 μl of 22 mg/ml $G\alpha_{i/12}$ with 1 μl well solution containing 100 mM sodium citrate pH 6.5, 50 mM NaCl, and 14% PEG 8000, and then suspending the drop over 1 ml of well solution at 4°C. Paper-thin, diamond shaped crystals appeared within one week. $G\alpha_{i/13}$ was crystallized similarly, except using 19 mg/ml $G\alpha_{i/13}$ and a well solution containing 100 mM sodium citrate (pH 4.8), 50 mM NaCl, and 10% PEG 2000. Tetragonal rod-shaped crystals appeared in 7 to 20 days. Both crystals were stabilized in a harvesting solution containing all the components of both the gel filtration buffer and their respective well solution, and were serially transferred, in 5% steps at a time, into a final concentration of 20% glycerol in harvesting solution. Crystals were then flash frozen in liquid nitrogen on nylon loops.

X-ray analysis and structure determination

Diffraction maxima were measured from crystals maintained at 100 K at the Advanced Photon Source beam line 17-ID using a Quantum 210 CCD detector. $G\alpha_{i/12}$ crystals exhibited severely anisotropic diffraction with disorder in the maxima that could have been due to warping of the extremely thin crystals. These defects, along with lower resolution diffraction limits, are probably responsible for the relatively high R-factors in the resulting model of $G\alpha_{i/12}$ compared to the $G\alpha_{i/13}$ structure (Table I). Data were reduced using HKL2000 (25). The space group choice and phase problem for $G\alpha_{i/13}$ was solved via molecular replacement with the program PHASER (26) using $G\alpha_{i1}$·GDP·AlF_4^- (PDB code: 1AGR) as the search model. The $G\alpha_{i/12}$ structure was determined using the partially refined $G\alpha_{i/13}$ structure as the search model. Each model was refined with several rounds of simulated annealing in CNS_SOLVE (27) and then restrained-refinement in REFMAC5 (28). Two-fold non-crystallographic symmetry restraints were used during refinement of $G\alpha_{i/12}$. Model building was performed with O (29). All reflections were used in the last round of refinement with final combined R-factors of 23.7% and 21.1% for the $G\alpha_{i/12}$·GDP·AlF_4^- and $G\alpha_{i/13}$·GDP structures, respectively. Coordinates and structure factors for the $G\alpha_{i/12}$ and $G\alpha_{i/13}$ structures are deposited at the PDB with accession codes 1ZCA and 1ZCB, respectively.

Miscellaneous procedures

GTPγS binding to $G\alpha_{i/13}$ or $G\alpha_{13}$ was measured by filter binding assays as described previously (23). Single-turnover GTP hydrolysis by $G\alpha_{i/13}$ or $G\alpha_{i/12}$ was analyzed in the absence (basal) or presence of 100 nM GST-p115-RH or GST-LARG-RH, as described previously for $G\alpha_{13}$ or $G\alpha_{12}$ (16). EE-tagged, full-length p115RhoGEF and $G\alpha_{13}$ were purified as described (24). Atomic representations were created with the program PYMOL (30).

Results and Discussion

Soluble expression of functional $G\alpha_{i/12}$ or $G\alpha_{i/13}$ in insect cells

To increase yields of functional $G\alpha_{12}$ or $G\alpha_{13}$, we constructed the $G\alpha_{i/12}$ and $G\alpha_{i/13}$ chimera, in which the N-terminal helices of mouse $G\alpha_{12}$ or $G\alpha_{13}$ were swapped with that of rat $G\alpha_{i1}$ (Fig. 1A and Figure S1). The $G\alpha_{i/13}$ chimera partitioned almost equally to the soluble and crude membrane fractions of Sf9 cells (data not shown). The soluble $G\alpha_{i/13}$ exhibited activation-dependent trypsin protection indicative of a functional Gα subunit (Fig. S2). Similar results were also obtained with $G\alpha_{i/12}$ (data not shown). The yield of $G\alpha_{i/13}$ was about 3.5 mg from 1 liter of Sf9 cell culture after Ni-NTA agarose chromatography (Fig. 1B), representing a vast improvement from previous methods (31). Similarly, the yield of $G\alpha_{i/12}$ was about 4.0 mg from 1 liter of culture (Fig. 1B). The expression of analogous chimeric proteins in *E. coli* resulted in large yields of soluble protein, but these proteins could not bind guanine nucleotides (data not shown).

$G\alpha_{i/12}$ and $G\alpha_{i/13}$ subunits bind guanine nucleotides and Gβγ

$G\alpha_{12/13}$ subunits possess biochemical properties that are distinct from those of most other Gα subunits. These include rates of nucleotide exchange (~0.01 min^{-1}) and GTP hydrolysis (~0.2 min^{-1}) that are roughly 3–10 fold slower than those of $G\alpha_s$ and $G\alpha_i$ subfamilies (20,21, 32). The activity of purified G$\alpha_{i/13}$ was evaluated by GTPγS binding assays. GTPγS binding to G$\alpha_{i/13}$ was effectively reduced in the presence of AlF_4^-, which was similar to control samples containing purified Gα_{i1} (Fig. S2). Furthermore, purified G$\alpha_{i/13}$ bound GTPγS with similar kinetics as wild-type Gα_{13} (Fig. 1C). G$\alpha_{i/12}$ also bound GTPγS similarly to wild-type Gα_{12} (data not shown). Because the N-terminal helix of Gα subunits is known to interact with G$\beta\gamma$ (33–35), we tested whether its substitution affected association of G$\alpha_{i/12}$ or G$\alpha_{i/13}$ with G$\beta\gamma$, as measured by the reduced binding of GTPγS to Gα in the presence of G$\beta\gamma$ (36). Assays performed in the presence of excess G$\beta\gamma$ showed marked inhibition of GTPγS binding to both chimeric proteins (Fig. 1D), indicating that G$\alpha_{i/12}$ and G$\alpha_{i/13}$ retain the ability to interact with G$\beta\gamma$.

RhoGEFs exhibit GAP activity for G$\alpha_{i/12}$ or G$\alpha_{i/13}$

Gα_{12} and Gα_{13} interact with the RH domain of p115RhoGEF or LARG in an AlF_4^--dependent manner (15,16). As shown in Figure 2, G$\alpha_{i/12}$ and G$\alpha_{i/13}$ also interacted with RH domain-containing fragments of p115RhoGEF or LARG in an AlF_4^--dependent manner, as assessed by GST pull-down assays. We also could isolate high affinity complexes of each chimeric G protein with the RH domain of LARG by size exclusion chromatography (data not shown). We next examined whether these same p115RhoGEF or LARG fragments exhibit GAP activity for the chimera. Both fragments accelerated the GTPase activity of G$\alpha_{i/12}$ and G$\alpha_{i/13}$ in single-turnover GTPase assays (Fig. 3A), with a faster response in G$\alpha_{i/13}$ than in G$\alpha_{i/12}$, as previously observed for their wild-type counterparts (15,16).

Regulation of RhoGEF activity by G$\alpha_{i/13}$ or G$\alpha_{i/12}$

Gα_{13}, but not Gα_{12}, directly stimulates p115RhoGEF-mediated nucleotide exchange on RhoA (13). To assess whether our chimera could similarly regulate RhoGEF activity, we measured GTPγS binding to RhoA in the presence of p115RhoGEF and AlF_4^--activated G$\alpha_{i/12}$ or G$\alpha_{i/13}$. As shown in Figure 3B, G$\alpha_{i/13}$, but not G$\alpha_{i/12}$, could stimulate p115RhoGEF. The dose-response curve of G$\alpha_{i/13}$ for p115RhoGEF activation is similar to that of wild-type Gα_{13} (Fig. 3C). Thus, G$\alpha_{i/12}$ and G$\alpha_{i/13}$ regulate effector molecules with specificity similar to their wild-type counterparts.

In summary, G$\alpha_{i/12}$ and G$\alpha_{i/13}$ chimeras retain the specific biochemical properties of their wild-type counterpart subunits. Although the N-terminal helices of Gα subunits are involved in binding G$\beta\gamma$ subunits, regulation of effector molecules, and specific interaction with receptors (33,37,38), substitution of the N-terminal helix of either Gα_{12} or Gα_{13} with that of Gα_{i1} did not affect its interaction with G$\beta\gamma$ or RhoGEFs insofar as our assays could detect. Thus, the native N-terminal helix of G$\alpha_{12/13}$, while important for receptor selectivity (38), is not essential for the regulation of RhoGEFs.

Structure determination of G$\alpha_{i/12}$ and G$\alpha_{i/13}$

Both G$\alpha_{i/12}$ and G$\alpha_{i/13}$ were activated with AlF_4^- prior to crystallization, and their structures were determined by molecular replacement (Table I). As is typical for structures of monomeric Gα subunits, the N-terminal helices and extreme C-termini are disordered. The structure of G$\alpha_{i/12}$·GDP·AlF_4^- spans residues 54 to 371, and therefore contains only wild-type residues (Fig. 4A). G$\alpha_{i/13}$ was resolved in a GDP-bound state that most closely resembles the deactivated structures of Gα_i and Gα_t (Fig. 4B, Fig. 5B). In its structure, only one residue derived from Gα_i at the chimeric N terminus is observed, and a portion of switch II (residues 226 to 232) and two residues in the α4-β6 loop (residues 339 to 340) are additionally disordered (Fig. 4B). It is somewhat surprising that the G$\alpha_{i/13}$ protein crystallized in a deactivated state because both G$\alpha_{i/12}$ and G$\alpha_{i/13}$ were activated using the same protocol, formed stable complexes with RH domains (Fig. 2) and were resistant to trypsin digestion (Fig. S2). However, AlF_4^- binding is reversible, and different crystallization conditions likely lead to different proportions of proteins in activated and deactivated states. The relatively low pH used for the crystallization of G$\alpha_{i/13}$ (pH 4.8), for example, could destabilize the activated, AlF_4^--bound state and allow the deactivated protein to crystallize (39). Previously reported Gα·AlF_4^- complexes were crystallized at pH values 5.5 or higher.

Comparison of the G$\alpha_{i/12}$ and G$\alpha_{i/13}$ structures

Like other Gα subunits, G$\alpha_{i/12}$ and G$\alpha_{i/13}$ are composed of a nucleotide-binding domain homologous to that of Ras, into which an α-helical domain is inserted (Fig. 4). The most dramatic difference between G$\alpha_{i/12}$·GDP·AlF_4^- and G$\alpha_{i/13}$·GDP is an ~8.5° rotation of the α-helical domain away from the Ras-like domain in G$\alpha_{i/13}$·GDP (Fig. 4C). Among previous Gα_i and Gα_t crystal structures, the Ras-like and α-helical domains differ in relative orientation only by ~2.5° between their activated and deactivated states. Thus, the G$\alpha_{i/13}$ structure is unusually "open" in conformation. This is most likely due to its activation state and not to differences in primary sequence between Gα_{12} and Gα_{13} (see below discussion).

In addition to the three switch regions, which are well known to exhibit activation-dependent conformational changes, the Ras-like domains of G$\alpha_{i/12}$ and G$\alpha_{i/13}$ exhibit differences in the α4-β6 loop, which is disordered and one residue longer in G$\alpha_{i/13}$. In other Gα subunits, this loop, along with the C-terminus, is thought to contribute to receptor specificity (reviewed in (40)). More subtle differences are also evident in the backbone of the α3-β5 loop, a region known to interact with effector proteins in Gα_s and Gα_t (4,41), although this could be affected by an effector-like crystal contact in the G$\alpha_{i/12}$ crystal lattice (Fig. S3). Excluding these regions, the Ras-like domains of G$\alpha_{i/12}$ and G$\alpha_{i/13}$ are quite similar, as might be expected by their 70% sequence identity. They superimpose with a root mean squared deviation (RMSD) of 0.75 Å for 175 equivalent C^α atoms (Fig. 4C).

The α-helical domains of G$\alpha_{i/12}$ and G$\alpha_{i/13}$ exhibit more profound differences. In G$\alpha_{i/13}$, the N-terminus of αA is kinked due to the presence of Pro86 (Asp93 in Gα_{12}), and the αB-αC loop is four residues longer and harbors an additional helix (αB1; Fig. 4B). Omitting these regions, the domains superimpose with an RMSD of 0.7 Å for 101 equivalent C^α atoms. Intriguingly, the αD-αE1 loop of G$\alpha_{i/13}$ (residues 171 to 173, immediately adjacent to the nucleotide binding site) adopts a strikingly different conformation from the analogous loops in the activated G$\alpha_{i/12}$ and G$\alpha_{13/i}$-5 structures, even though these loops have identical primary structure (Fig. 5A, 5B). Therefore, the αD-αE1 loop also appears to exhibit a novel activation-dependent conformational change.

Comparison of G$\alpha_{12/13}$ subunits with other Gα subfamilies

In line with their sequence identities (43% and 39%, respectively), the Ras-like domains of G$\alpha_{12/13}$ are more similar to Gα_i than Gα_s, with RMSDs of superposition of 1.1 Å and 2.2 Å for 184 and 170 equivalent C^α atoms, respectively. Regions exhibiting obvious structural differences among the Ras-like domains of G$\alpha_{12/13}$, Gα_i, and Gα_s are the α4-β6 loop, which projects further away from the Ras-like domain in G$\alpha_{12/13}$ subunits, and the β5-α4 loop (Fig. 4C). The cleft formed between the α2 (switch II) and α3 helices and their C-terminal loops is increasingly recognized as the effector binding site of Gα (17,41,42). In G$\alpha_{12/13}$ subunits, the α3-β5 loop is most similar to that of Gα_t. Differences between the α-helical domains of G$\alpha_{12/13}$ and Gα subunits from other subfamilies have been described previously (17).

Activation-Dependent Conformational changes in G$\alpha_{12/13}$ subunits

Comparison of the structures of G$\alpha_{i/12}$·GDP·AlF_4^-, G$\alpha_{i/13}$·GDP and G$\alpha_{13/i}$-5·GDP·AlF_4^- reveals conformational changes that appear to be linked to GTP hydrolysis in G$\alpha_{12/13}$ subunits (Fig. 4 and Movie S1). This important deactivation mechanism has previously only been described for the Gα_i subfamily of G proteins. In the G$\alpha_{i/12}$·GDP·AlF_4^- structure, the three switch regions and the α-helical domain adopt a conformation similar to those of the activated structures of $G\alpha_i$, $G\alpha_t$ and $G\alpha_s$. In $G\alpha_{i/13}$·GDP, switch I retains this activated conformation except for residues 206 to 210 at the C terminus of the switch, which shift by as much as 2 Å towards the α-helical domain (Fig. 4C), a conformation previously observed in several GDP-bound structures of $G\alpha_i$ (34,43). Less of switch II is disordered in the $G\alpha_{i/13}$·GDP structure than in $G\alpha_{i1}$·GDP, and switch III rotates 13° away from the active site to a position nearly identical to that observed in the $G\alpha_t$·GDP complex (44).

As described above, the α-helical domain of $G\alpha_{i/13}$ also appears to undergo activation-dependent conformational changes (Fig. 4C, 5B) by rotating away from the Ras-like domain and by alteration of the αD-αE1 loop (residues 171 to 173 in $G\alpha_{i/13}$). In other subfamilies, $G\alpha_{13}$-Glu172 is substituted by aspartate, which interacts with an invariant lysine in the Ras-like domain ($G\alpha_{13}$-Lys292) and packs against the purine ring and ribose sugar of GDP. The unusually open conformation of $G\alpha_{i/13}$·GDP allows the longer $G\alpha_{13}$-Glu172 side chain to form an analogous salt bridge (Fig. 5A), although in electron density maps this side chain appears less ordered than its neighboring residues. Contrarily, in activated structures of $G\alpha_{12}$ and $G\alpha_{13/i}$-5, the αD-αE1 loop is puckered, apparently to avoid steric collisions, and $G\alpha_{13}$-Glu172 makes relatively few contacts with the bound nucleotide (Fig. 5). Thus, the αD-αE1 loop thus acts like an activation-dependent "spring" that appears to push the α-helical domain away from the Ras-like domain in the $G\alpha_{i/13}$·GDP structure. This transition may be facilitated by the loss of contacts between the α-helical domain and switch III upon GTP hydrolysis.

To better understand whether these conformational differences are coupled to GTP hydrolysis and not to differences in primary structure, we need atomic structures of the activated and deactivated forms of both $G\alpha_{i/12}$ and $G\alpha_{i/13}$. Currently, $G\alpha_{i/12}$·GDP has not been crystallized, and we only have the $G\alpha_{13/i}$-5 chimera to represent the activated structure of $G\alpha_{13}$. Despite this, the 70% sequence identity of $G\alpha_{12}$ and $G\alpha_{13}$ and the 100% identity of their αD-αE1 loops suggest that they undergo similar conformational changes upon deactivation. Indeed, the activated structures of $G\alpha_{i/12}$ and the $G\alpha_{13/i}$-5 chimera are remarkably similar despite their even higher sequence disparity. Furthermore, in the $G\alpha_{i/13}$·GDP structure, the αD-αE1 loop adopts the same conformation as those of activated and deactivated structures of $G\alpha_i$, $G\alpha_t$ and $G\alpha_s$, suggesting that this is the energetically preferred state, which can only be attained in $G\alpha_{12/13}$ subunits after GTP hydrolysis and outward rotation of the helical domain. However, as in any crystal structure, we cannot totally exclude the possibility that the unusually open conformation of the $G\alpha_{i/13}$·GDP structure was also influenced by lattice contacts or crystallization conditions.

If the open conformation of the $G\alpha_{i/13}$·GDP structure and the structural transition of the αD-αE1 loop indeed represent activation-dependent conformational changes in $G\alpha_{12/13}$ subunits, what might their physiological significance be? Because the Ras-like and α-helical domains of $G\alpha_{13}$ are both known to interact with the N-terminal fragment p115RhoGEF (17), the open conformation of deactivated $G\alpha_{i/13}$·GDP could help discourage interactions with p115RhoGEF or LARG upon GTP hydrolysis. Another consequence of the open conformation of $G\alpha_{i/13}$·GDP is that the nucleotide appears less solvent accessible in deactivated $G\alpha_{i/13}$ than in activated $G\alpha_{12/13}$ subunits (~14.5 Å^2 of accessible surface area in the $G\alpha_{i/12}$·GDP·AlF_4^- and $G\alpha_{13/i}$-5·GDP·AlF_4^- complexes, and 6.9 Å^2 in the $G\alpha_{i/13}$·GDP complex). The opposite is true in $G\alpha_i$ subunits (*e.g.* 18.8 Å^2 in the structure of $G\alpha_i$·GDP, and 3.5 Å^2 in $G\alpha_i$·GDP·AlF_4^-). These differences in the substrate binding site could influence rates of nucleotide exchange and/or hydrolysis, and thus the duration of signals in response to the activation of $G\alpha_{12/13}$-coupled receptors.

Structural insights into the interactions of Gα_{12} and Gα_{13} with effectors

The best-characterized G$\alpha_{12/13}$ effector is the N-terminal fragment of p115RhoGEF, which includes its RH domain (17). Because the G$\alpha_{13/i}$-5-p115RhoGEF structure determination employed a Gα subunit with a chimeric effector-binding site, we modeled the p115RhoGEF RH domain complex with our essentially wild-type G$\alpha_{i/13}$ and G$\alpha_{i/12}$ structures. The resulting model reveals that the chimeric residues in the G$\alpha_{13/i}$-5-p115RhoGEF interface either do not make significant contributions or are conservatively substituted in G$\alpha_{i/13}$ and G$\alpha_{i/12}$. In line with our observation that the RH domains of p115RhoGEF and LARG bind G$\alpha_{i/12}$ and G$\alpha_{i/13}$ equally well (Fig. 2), the structures of G$\alpha_{i/12}$ and G$\alpha_{i/13}$ have no significant amino acid differences among the residues that contribute to their respective RH domain binding sites. However, Gα_{12} and Gα_{13} subunits do exhibit differences in their GAP response to p115RhoGEF and LARG. The region immediately N-terminal to the RH domain of p115RhoGEF is responsible for its GAP activity and binds in the cleft formed between the Ras-like and α-helical domains (17,19), where it contacts αA and the αB-αC loop. While the interacting residues within αA are conserved in Gα_{12} and Gα_{13}, their αB-αC loops have dramatically different structure (Fig. 4). Diminished or detrimental interactions between the shorter αB-αC loop of G$\alpha_{i/12}$ and p115RhoGEF could therefore account for the higher GAP response of G$\alpha_{i/13}$ with respect to G$\alpha_{i/12}$.

Another relatively-well characterized effector target of activated G$\alpha_{12/13}$ subunits is cadherin (10). Recently, it was shown that mutation of residues 244 to 249 within β4 of Gα_{12} lead to uncoupling of Gα_{12} from p115RhoGEF and LARG, but not E-cadherin (45). Based on the crystal structure of G$\alpha_{i/12}$, this substitution is expected to disrupt the effector-binding site of the G protein, in accordance with the loss of p115RhoGEF and LARG binding. Cadherin either binds elsewhere on G$\alpha_{i/12}$, or is less reliant on a properly structured effector-binding pocket.

Conclusions

Elucidation of the molecular mechanisms by which Gα subunits regulate their own activity as well as the activity of their effector target is required not only to understand the regulation of many cellular processes, but also to develop drugs designed to modulate such processes. Gα_{12} and Gα_{13} have similar biochemical properties (20,21), but distinct functional roles in cell signaling, such that Gα_{13} knockout mice die around embryonic day E10 due to a vascular system formation defect (46), whereas Gα_{12} knockout mice are viable and without any obvious phenotype (47). In this study, we demonstrate a simple and efficient method to produce fully functional, soluble forms of Gα_{12} and Gα_{13} that enabled us to determine their crystal structures. These structures reveal molecular differences not only between these two subunits, but also with those of other Gα subunits. By determining the activated structure of Gα_{12} and the deactivated structure of Gα_{13}, we fortuitously observed novel conformational changes that are likely coupled to GTP hydrolysis. If true, then it can no longer be assumed that the transition upon deactivation will necessarily be the same in all Gα subfamilies. In the future, these chimeric subunits can be used in biochemical and crystallographic analyses to decipher their differential ability to regulate the growing number of effectors that interact with G$\alpha_{12/13}$ subunits (12). Remarkably, the chimeric approach we used to generate soluble G$\alpha_{12/13}$ subunits in this paper can be applied successfully to other, formerly intractable Gα subunits, even from other subfamilies, as evidenced by our successful structural studies of the analogous G$\alpha_{i/q}$ chimera in complex with GRK2 and Gβγ (48).

Supplementary Material

Refer to Web version on PubMed Central for supplementary material.

Abbreviations

βME, β-mercaptoethanol
DTT, dithiothreitol
EDTA, ethylenediaminetetraacetic acid
G protein, guanine nucleotide binding protein
Gα, heterotrimeric G protein α subunit
Gβγ, heterotrimeric G protein β and γ subunits
GPCR, G protein-coupled receptor
GDP, guanosine-5'-diphosphate
GST, glutathione-*S*-transferase
GTP, guanosine-5'-triphosphate
HEPES, 4-(2-hydroxyethyl)-1-piperazine ethanesulfonic acid
LARG, leukemia-associated RhoGEF
p115RhoGEF, p115 Rho guanine nucleotide exchange factor
RGS, regulator of G protein signaling
RH, RGS homology
SDS, sodium dodecyl sulfate

Acknowledgments

We would like to thank Yi Li and Beth Dulin for technical assistance. Diffraction data were collected at beam line 17-ID of the Industrial Macromolecular Crystallography Association Collaborative Access Team (IMCA-CAT) at the Advanced Photon Source (Argonne, IL). These facilities are supported by the companies of the Industrial Macromolecular Crystallography Association through a contract with Illinois Institute of Technology (IIT), executed through the IIT Center for Synchrotron Radiation Research and Instrumentation. Use of the Advanced Photon Source was supported by the U. S. Department of Energy, Basic Energy Sciences, Office of Science, under Contract No. W-31-109-Eng-38.

References

1. Neves SR, Ram PT, Iyengar R. G protein pathways. Science 2002;296:1636–1639. [PubMed: 12040175]
2. Hollinger S, Hepler JR. Cellular regulation of RGS proteins: modulators and integrators of G protein signaling. Pharmacol Rev 2002;54:527–559. [PubMed: 12223533]
3. Berman DM, Kozasa T, Gilman AG. The GTPase-activating protein RGS4 stabilizes the transition state for nucleotide hydrolysis. J Biol Chem 1996;271:27209–27212. [PubMed: 8910288]
4. Tesmer JJG, Berman DM, Gilman AG, Sprang SR. Structure of RGS4 bound to AlF_4^--activated $G_{i\alpha1}$: stabilization of the transition state for GTP hydrolysis. Cell 1997;89:251–261. [PubMed: 9108480]
5. Hepler JR, Gilman AG. G proteins. Trends Biochem Sci 1992;17:383–387. [PubMed: 1455506]
6. Dhanasekaran N, Dermott JM. Signaling by the G_{12} class of G proteins. Cell Signal 1996;8:235–245. [PubMed: 8842523]
7. Whitehead IP, Zohn IE, Der CJ. Rho GTPase-dependent transformation by G protein-coupled receptors. Oncogene 2001;20:1547–1555. [PubMed: 11313901]
8. Sah VP, Seasholtz TM, Sagi SA, Brown JH. The role of Rho in G protein-coupled receptor signal transduction. Annu Rev Pharmacol Toxicol 2000;40:459–489. [PubMed: 10836144]
9. Sahai E, Marshall CJ. RHO-GTPases and cancer. Nat Rev Cancer 2002;2:133–142. [PubMed: 12635176]
10. Meigs TE, Fields TA, McKee DD, Casey PJ. Interaction of $G\alpha_{12}$ and $G\alpha_{13}$ with the cytoplasmic domain of cadherin provides a mechanism for β-catenin release. Proc Natl Acad Sci U S A 2001;98:519–524. [PubMed: 11136230]
11. Yamaguchi Y, Katoh H, Mori K, Negishi M. $G\alpha_{12}$ and $G\alpha_{13}$ interact with Ser/Thr protein phosphatase type 5 and stimulate its phosphatase activity. Curr Biol 2002;12:1353–1358. [PubMed: 12176367]

12. Kurose H. $G\alpha_{12}$ and $G\alpha_{13}$ as key regulatory mediator in signal transduction. Life Sci 2003;74:155–161. [PubMed: 14607242]

13. Hart MJ, Jiang X, Kozasa T, Roscoe W, Singer WD, Gilman AG, Sternweis PC, Bollag G. Direct stimulation of the guanine nucleotide exchange activity of p115 RhoGEF by $G\alpha_{13}$. Science 1998;280:2112–2114. [PubMed: 9641916]

14. Fukuhara S, Murga C, Zohar M, Igishi T, Gutkind JS. A novel PDZ domain containing guanine nucleotide exchange factor links heterotrimeric G proteins to Rho. J Biol Chem 1999;274:5868–5879. [PubMed: 10026210]

15. Suzuki N, Nakamura S, Mano H, Kozasa T. $G\alpha_{12}$ activates Rho GTPase through tyrosine-phosphorylated leukemia-associated RhoGEF. Proc Natl Acad Sci U S A 2003;100:733–738. [PubMed: 12515866]

16. Kozasa T, Jiang X, Hart MJ, Sternweis PM, Singer WD, Gilman AG, Bollag G, Sternweis PC. p115 RhoGEF, a GTPase activating protein for $G\alpha_{12}$ and $G\alpha_{13}$. Science 1998;280:2109–2111. [PubMed: 9641915]

17. Chen Z, Singer WD, Sternweis PC, Sprang SR. Structure of the p115RhoGEF rgRGS domain-$G\alpha_{13/i1}$ chimera complex suggests convergent evolution of a GTPase activator. Nat Struct Mol Biol 2005;12:191–197. [PubMed: 15665872]

18. Chen Z, Singer WD, Wells CD, Sprang SR, Sternweis PC. Mapping the $G\alpha_{13}$ binding interface of the rgRGS domain of p115RhoGEF. J Biol Chem 2003;278:9912–9919. [PubMed: 12525488]

19. Wells CD, Liu MY, Jackson M, Gutowski S, Sternweis PM, Rothstein JD, Kozasa T, Sternweis PC. Mechanisms for reversible regulation between G_{13} and Rho exchange factors. J Biol Chem 2002;277:1174–1181. [PubMed: 11698392]

20. Kozasa T, Gilman A. Purification of recombinant G proteins from Sf9 cells by hexahistidine tagging of associated subunits. Characterization of α_{12} and inhibition of adenylyl cyclase by α_z. J Biol Chem 1995;270:1734–1741. [PubMed: 7829508]

21. Singer WD, Miller RT, Sternweis PC. Purification and characterization of the α subunit of G_{13}. J Biol Chem 1994;269:19796–19802. [PubMed: 8051060]

22. Yasukawa T, Kanei-Ishii C, Maekawa T, Fujimoto J, Yamamoto T, Ishii S. Increase of solubility of foreign proteins in *Escherichia coli* by coproduction of the bacterial thioredoxin. J Biol Chem 1995;270:25328–25331. [PubMed: 7592692]

23. Nakamura S, Kreutz B, Tanabe S, Suzuki N, Kozasa T. Critical role of lysine 204 in switch I region of $G\alpha_{13}$ for regulation of p115RhoGEF and leukemia-associated RhoGEF. Mol Pharmacol 2004;66:1029–1034. [PubMed: 15258251]

24. Tanabe S, Kreutz B, Suzuki N, Kozasa T. Regulation of RGS-RhoGEFs by $G\alpha_{12}$ and $G\alpha_{13}$ proteins. Methods Enzymol 2004;390:285–294. [PubMed: 15488184]

25. Otwinoski Z, Minor W. Processing of X-ray diffraction data collected in oscillation mode. Methods Enzymol 1997;276:307–326.

26. Storoni LC, McCoy AJ, Read RJ. Likelihood-enhanced fast rotation functions. Acta Crystallogr D Biol Crystallogr 2004;60:432–438. [PubMed: 14993666]

27. Brünger AT, Adams PD, Clore GM, DeLano WL, Gros P, Grosse-Kunstleve RW, Jiang JS, Kuszewski J, Nilges M, Pannu NS, Read RJ, Rice LM, Simonson T, Warren GL. Crystallography & NMR system: A new software suite for macromolecular structure determination. Acta Crystallogr D Biol Crystallogr 1998;54:905–921. [PubMed: 9757107]

28. Winn MD. An overview of the CCP4 project in protein crystallography: an example of a collaborative project. J Synchrotron Radiat 2003;10:23–25. [PubMed: 12511787]

29. Jones TA, Zou JY, Cowan SW, Kjeldgaard M. Improved methods for the building of protein models in electron density maps and the location of errors in these models. Acta Crystallogr 1991;A47:110–119.

30. DeLano, W. The PyMOL Molecular Graphics System. San Carlos, CA, USA: DeLano Scientific; 2002.

31. Kozasa T. Purification of G protein subunits from Sf9 insect cells using hexahistidine-tagged α and βγ subunits. Methods Mol Biol 2004;237:21–38. [PubMed: 14501036]

32. Linder M, Ewald D, Miller R, Gilman A. Purification and characterization of $G_{o\alpha}$ and three types of $G_{i\alpha}$ after expression in Escherichia coli. J Biol Chem 1990;265:8243–8251. [PubMed: 2159473]

33. Neer EJ, Pulsifer L, Wolf LG. The amino terminus of G protein α subunits is required for interaction with βγ. J Biol Chem 1988;263:8996-70. [PubMed: 3132454]

34. Wall MA, Coleman DE, Lee E, Iniguez-Lluhi JA, Posner BA, Gilman AG, Sprang SR. The structure of the G protein heterotrimer $G_{i\alpha1}\beta_1\gamma_2$. Cell 1995;83:1047–1058. [PubMed: 8521505]

35. Lambright DG, Sondek J, Bohm A, Skiba NP, Hamm HE, Sigler PB. The 2.0 A crystal structure of a heterotrimeric G protein. Nature 1996;379:311–319. [PubMed: 8552184]

36. Brandt DR, Ross EM. GTPase activity of the stimulatory GTP-binding regulatory protein of adenylate cyclase, G_s. Accumulation and turnover of enzyme-nucleotide intermediates. J Biol Chem 1985;260:266–272. [PubMed: 2981206]

37. Hepler JR, Biddlecome GH, Kleuss C, Camp LA, Hofmann SL, Ross EM, Gilman AG. Functional importance of the amino terminus of $G_{q\alpha}$. J Biol Chem 1996;271:496–504. [PubMed: 8550609]

38. Yamaguchi Y, Katoh H, Negishi M. N-terminal short sequences of α subunits of the G_{12} family determine selective coupling to receptors. J Biol Chem 2003;278:14936–14939. [PubMed: 12594220]

39. Schlichting I, Reinstein J. pH influences fluoride coordination number of the AlFx phosphoryl transfer transition state analog. Nat Struct Biol 1999;6:721–723. [PubMed: 10426946]

40. Cabrera-Vera TM, Vanhauwe J, Thomas TO, Medkova M, Preininger A, Mazzoni MR, Hamm HE. Insights into G protein structure, function, and regulation. Endocr Rev 2003;24:765–781. [PubMed: 14671004]

41. Slep KC, Kercher MA, He W, Cowan CW, Wensel TG, Sigler PB. Structural determinants for regulation of phosphodiesterase by a G protein at 2.0 Å. Nature 2001;409:1071–1077. [PubMed: 11234020]

42. Tesmer J, Sunahara R, Gilman A, Sprang S. Crystal structure of the catalytic domains of adenylyl cyclase in a complex with $G_{s\alpha}$·GTPγS. Science 1997;278:1907–1916. [PubMed: 9417641]

43. Kimple RJ, Kimple ME, Betts L, Sondek J, Siderovski DP. Structural determinants for GoLoco-induced inhibition of nucleotide release by Gα subunits. Nature 2002;416:878–881. [PubMed: 11976690]

44. Lambright DG, Noel JP, Hamm HE, Sigler PB. Structural determinants for activation of the α-subunit of a heterotrimeric G protein. Nature 1994;369:621–628. [PubMed: 8208289]

45. Meigs TE, Juneja J, Demarco CT, Stemmle LN, Kaplan DD, Casey PJ. Selective uncoupling of $G\alpha_{12}$ from Rho-mediated signaling. J Biol Chem 2005;280:18049–18055. [PubMed: 15746095]

46. Offermanns S, Mancino V, Revel JP, Simon MI. Vascular system defects and impaired cell chemokinesis as a result of $G\alpha_{13}$ deficiency. Science 1997;275:533–536. [PubMed: 8999798]

47. Gu JL, Muller S, Mancino V, Offermanns S, Simon MI. Interaction of $G\alpha_{12}$ with $G\alpha_{13}$ and $G\alpha_q$ signaling pathways. Proc Natl Acad Sci U S A 2002;99:9352–9357. [PubMed: 12077299]

48. Tesmer V, Kawano T, Shankaranarayanan A, Kozasa T, Tesmer JJG. Snapshot of activated G proteins at the membrane: the $G\alpha_q$-GRK2-Gβγ complex. Science. 2005In press

NIH-PA Author Manuscript

NIH-PA Author Manuscript

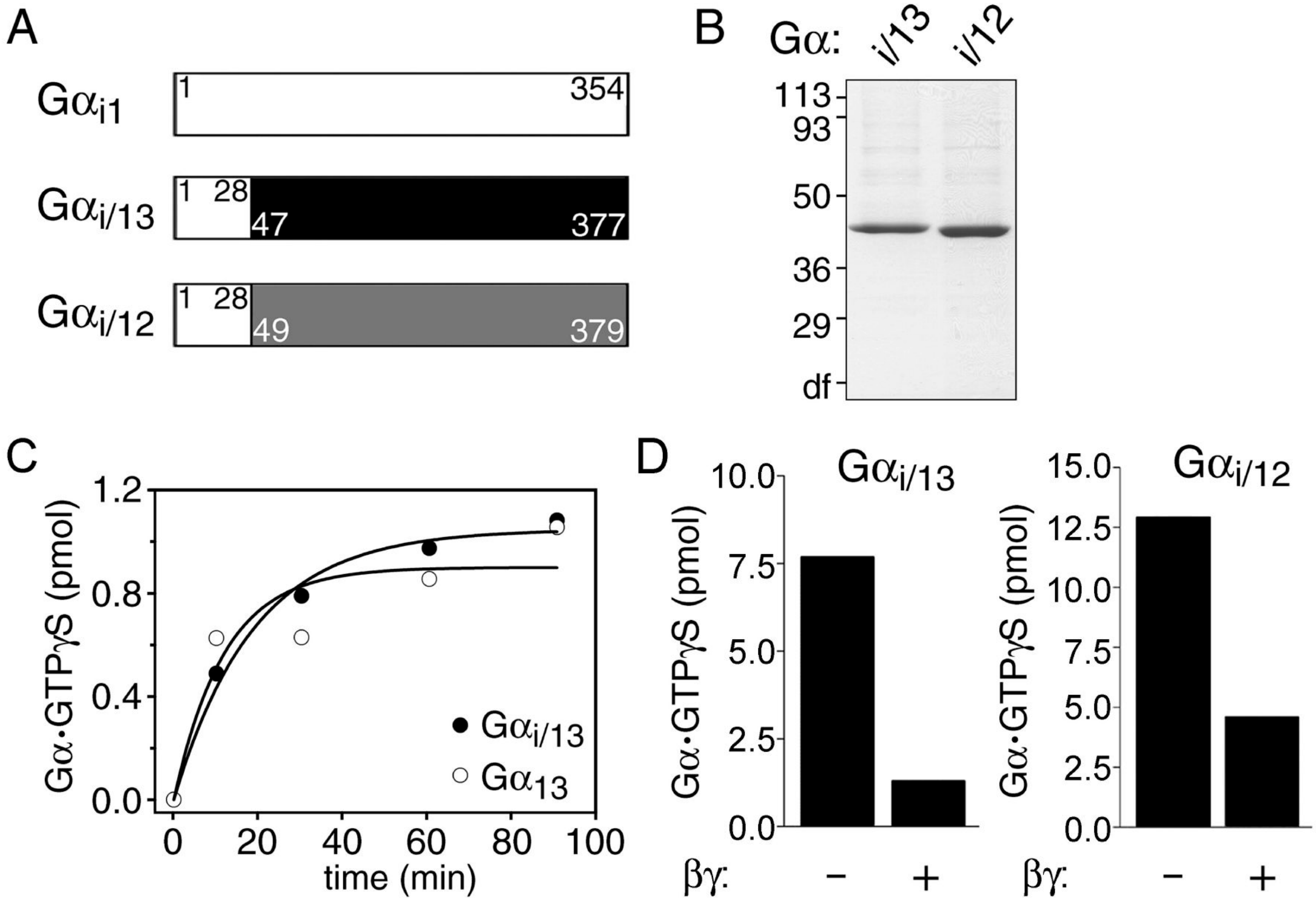

Figure 1.

Generation of $G\alpha_{i/13}$ and $G\alpha_{i/12}$ chimeric proteins. (A) Schematic representation of the $G\alpha_{i/13}$ and $G\alpha_{i/12}$ chimera. Residues of $G\alpha_{i1}$ are shown in white, and numbers within the colored regions of the $G\alpha_{i/13}$ or $G\alpha_{i/12}$ chimera correspond to original numbering of residues contributed by $G\alpha_{13}$ (black) or $G\alpha_{12}$ (gray). (B) Purified His_6-$G\alpha_{i/13}$ or His_6-$G\alpha_{i/12}$ (3 μg) were subjected to SDS-PAGE and stained with Coomassie Brilliant Blue. The position and apparent molecular weight of standard proteins (in kDa) is indicated. (C) GTPγS binding to $G\alpha_{i/13}$ (●) or wild-type $G\alpha_{13}$ (○) was measured at 30°C. Data are the mean of duplicate determinations. (D) $G\alpha_{i/13}$ or $G\alpha_{i/12}$ functionally interact with Gβγ. GTPγS binding to $G\alpha_{i/13}$ or $G\alpha_{i/12}$ (3 μg each) was measured either in the absence or presence of Gβγ (20 μg) as indicated. GTPγS binding was quantified after 90 min at 30°C. Data are the mean of duplicate determinations.

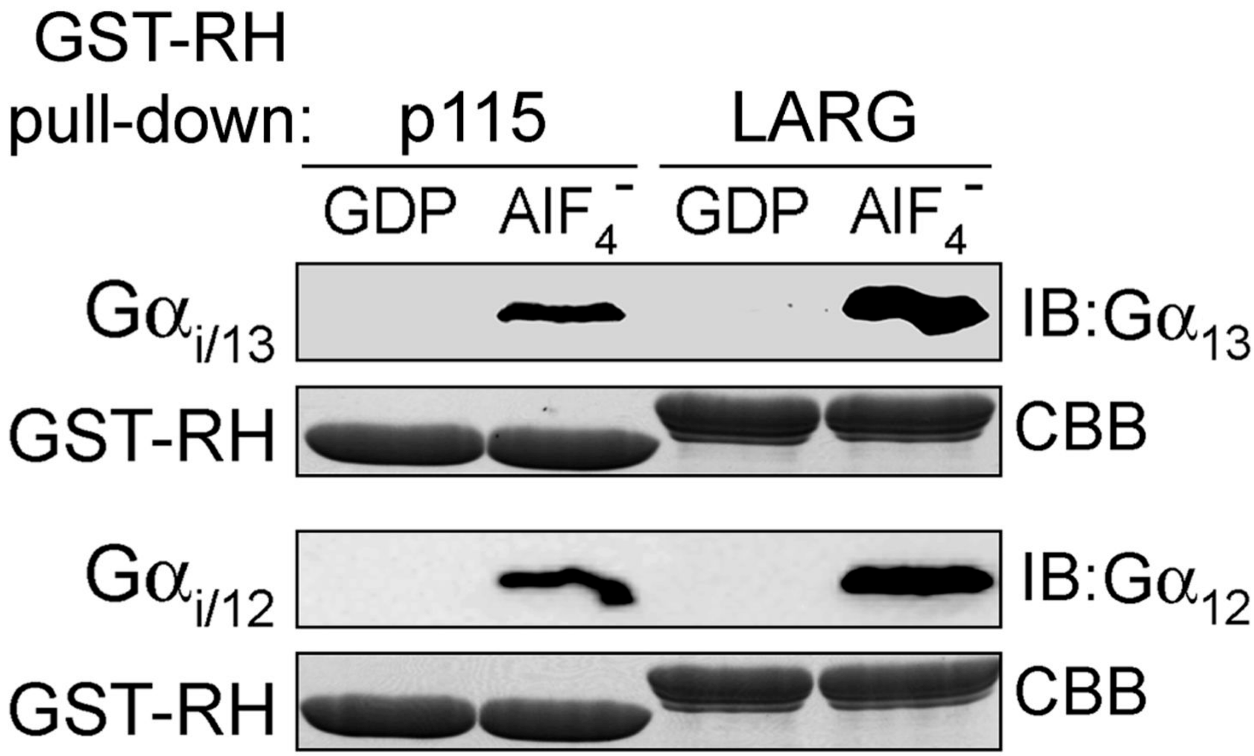

Figure 2.

$G\alpha_{i/13}$ or $G\alpha_{i/12}$ chimera interact with RH domains in an activation-dependent manner. GST-p115-RH or GST-LARG-RH were incubated with purified His_6-$G\alpha_{i/13}$ (upper panels) or His_6-$G\alpha_{i/12}$ (lower panels), either in the absence or presence of AlF_4^-, and then GST-RH was pulled down using glutathione Sepharose 4B resin. Protein eluted from washed beads was resolved by SDS-PAGE and either immunoblotted (IB) with anti-$G\alpha_{13}$ (B860) or anti-$G\alpha_{12}$ (J168) antibody, or stained by Coomassie Brilliant Blue (CBB).

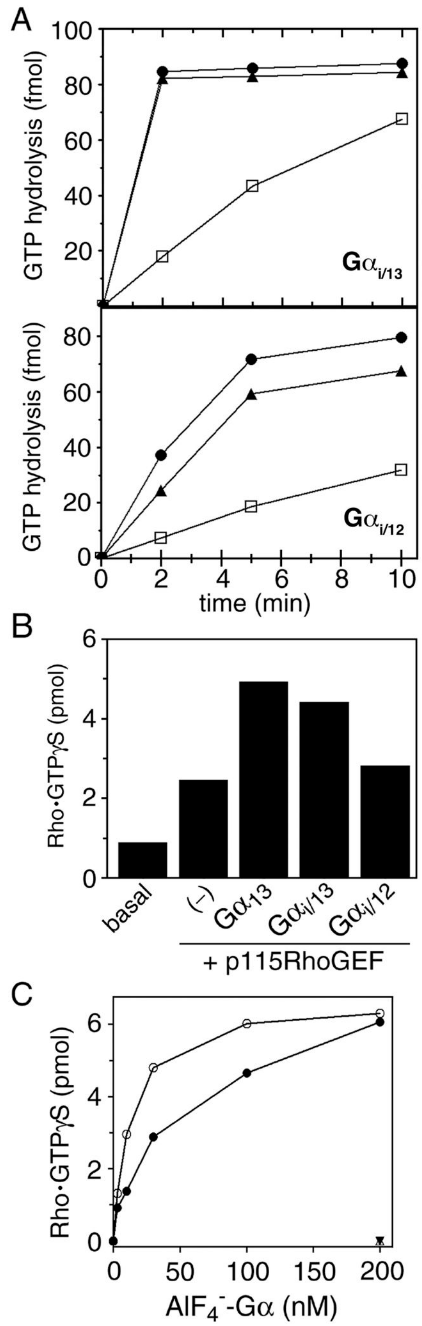

Figure 3.

Activity of purified $G\alpha_{i/13}$ and $G\alpha_{i/12}$ in reconstitution assays. (A) Single-turnover hydrolysis of GTP bound to $G\alpha_{i/13}$ (upper panel) or $G\alpha_{i/12}$ (lower panel) was measured at 15°C in the absence (□) or presence of 100 nM GST-p115-RH (●) or 100 nM GST-LARG-RH (▲). Data are from one experiment, which is representative of three experiments. (B) Stimulation of p115RhoGEF activity by $G\alpha_{i/13}$ but not $G\alpha_{i/12}$. GTPγS binding to His_6-RhoA was measured after incubation for 5 min at 30°C in the presence of p115RhoGEF (5 nM) and indicated AlF_4^--activated Gα subunit (100 nM). Data are the mean of duplicate determinations from one experiment, which is representative of three experiments. (C) Dose-dependent stimulation of p115RhoGEF activity by $G\alpha_{i/13}$. GTPγS binding to His_6-RhoA by p115RhoGEF (5 nM) was evaluated after 5 min at 30°C, and included the indicated concentration of either AlF_4^--activated wild-type $G\alpha_{13}$ (○) or $G\alpha_{i/13}$ (●). Samples lacking RhoA but containing p115RhoGEF and either AlF_4^--activated wild-type $G\alpha_{13}$ (△) or $G\alpha_{i/13}$ (▼) were assayed in parallel.

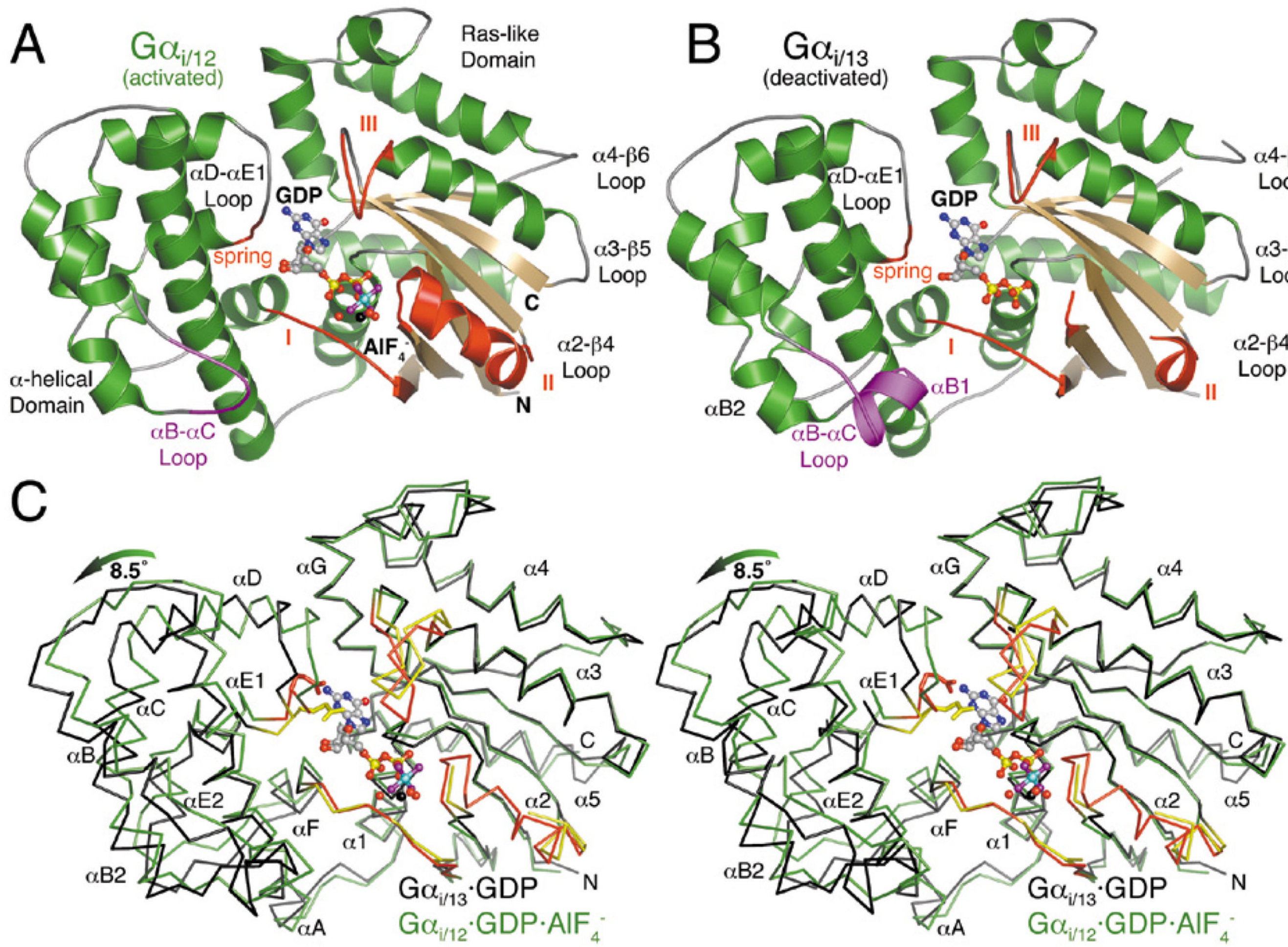

Figure 4.

Structures of Gα$_{12/13}$ subunits in activated and deactivated states. (A) The activated Gα$_{i/12}$·GDP·AlF$_4^-$ complex. The region of the αB-αC loop distinct from that of Gα$_{i/13}$ is colored purple. The three conformationally flexible "switch regions" of the Gα subunit are red and labeled with Roman numerals (I–III). A fourth, apparently Gα$_{12/13}$-specific element (the "spring") is likewise colored red. The Mg^{2+}·GDP·AlF$_4^-$ ligand complex is shown as a ball-and-stick model, with carbons colored gray, oxygens red, nitrogens blue, phosphates yellow, fluorines purple, aluminum cyan and magnesium black. Waters are shown as red spheres. (B) The deactivated Gα$_{i/13}$·GDP complex adopts an unusually open conformation in which the α-helical domain has rotated ~8.5° away from the Ras-like domain. Switch II is almost completely disordered, and switch III has rotated away (up in the figure) from the nucleotide binding site. (C) Stereo view of the C^{α} traces of Gα$_{i/12}$·GDP·AlF$_4^-$ (green with red switch regions) and Gα$_{i/13}$·GDP (black with yellow switch regions), superimposed using their Ras-like domains. The glutamate side chain in the "spring" of each α-helical domain (E175 in Gα$_{12}$, E172 in Gα$_{13}$) is shown as a stick model.

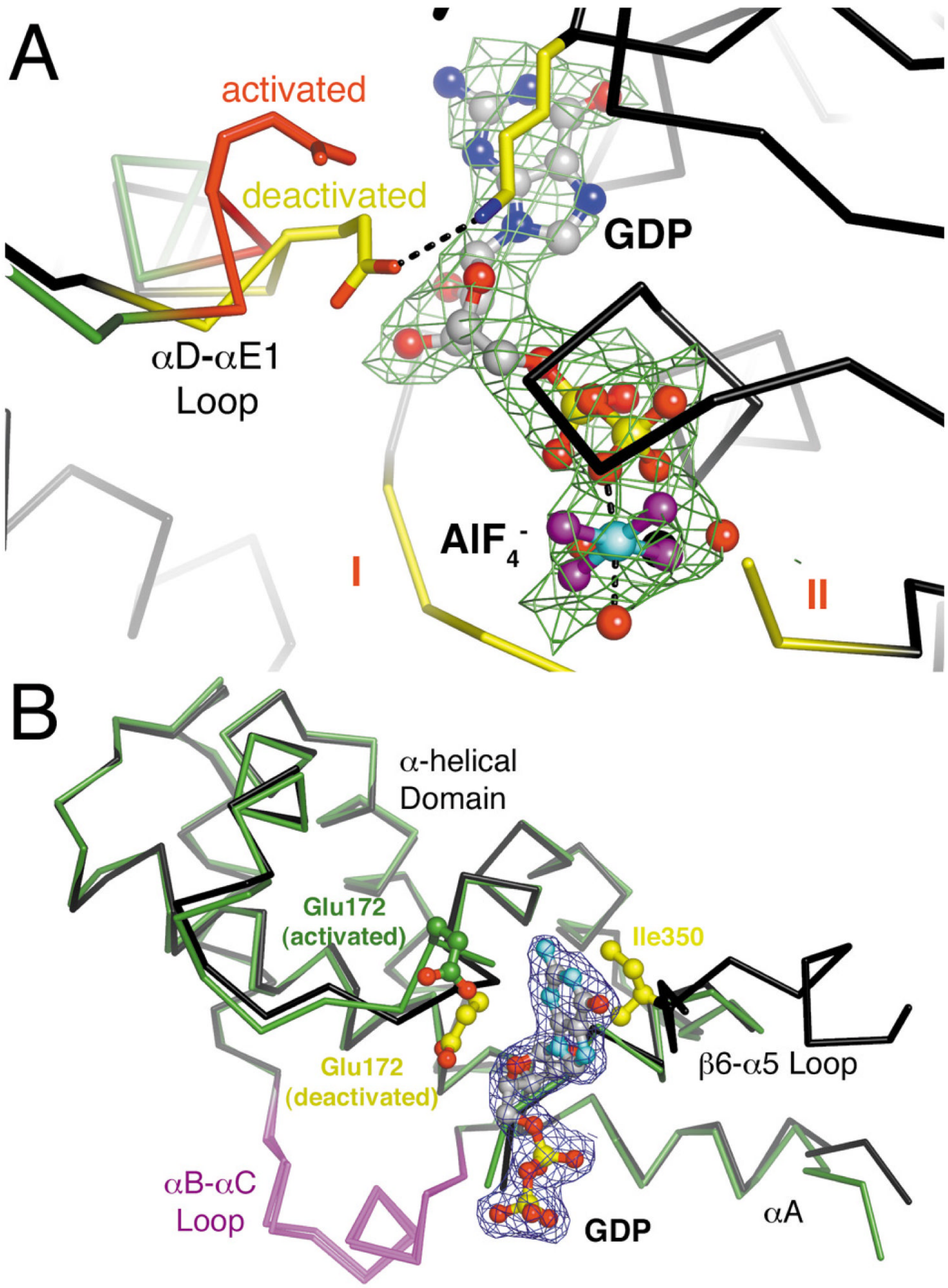

Figure 5.

The active sites and α-helical domains of activated and deactivated $G\alpha_{12/13}$ subunits. (A) The activation-dependent "spring" of the α-helical domain. In the deactivated (GDP-bound) state, $G\alpha_{i/13}$-E172 (yellow) is extended to form a salt bridge with Lys292 and packs against the nucleotide. In the activated (AlF_4^--bound) state, the spring (red) adopts a curled conformation and $G\alpha_{i/12}$-Glu175 does not contact the bound nucleotide. Only the Ras-like domain of $G\alpha_{i/13}$ is shown for clarity. Electron density from a 2.5 σ $|F_o|$-$|F_c|$ omit map from the $G\alpha_{i/12}$·GDP·AlF_4^- crystal structure is shown as green wire cage. (B) Superposition of the activated and deactivated conformations of the $G\alpha_{13}$ α-helical domain. The C^{α}-trace of the α-helical domain (residues 74 to 201) and the β6-α5 loop (residues 345 to 357) of the

$G\alpha_{i/13}$·GDP structure are colored black, and the α-helical domain from the $G\alpha_{13/i}$-5·p115RhoGEF complex is colored green. The αD-αE1 loop in the α-helical domain and the linker between the Ras-like and α-helical domains (N-terminal to αA) exhibit the most profound conformational changes upon nucleotide hydrolysis. Electron density from a 1.0 σ $2|F_o|-|F_c|$ map derived from the $G\alpha_{i/13}$·GDP crystal structure is shown as green wire cage.

NIH-PA Author Manuscript

NIH-PA Author Manuscript

Table I

Crystallographic data and refinement statistics

X-ray Source: APS 17-ID	**G$\alpha_{i/12}$·GDP·AlF_4^-**	**G$\alpha_{i/13}$·GDP**
Wavelength (Å)	1.000	1.000
D_{min} (Å)	2.9[a]	2.0
Space group	$P2_1$	$P4_32_12$
Cell constants (Å, °)	a = 57.5, b = 85.2, c = 82.9; β = 106.1, α = γ = 90	a = b = 67.4, c = 175.2; α = β = γ = 90
Unique reflections	15263 (1140)[c]	27297 (2761)[c]
Average redundancy	2.5 (1.7)	5.7 (4.0)
R_{sym} (%)[b]	10.2 (29.6)	4.9 (38.5)
Completeness (%)	88.7 (67.4)	96.7 (100)
$\langle I\rangle/\langle\sigma_I\rangle$	6.9 (1.7)	42.6 (3.4)
Refinement resolution (Å)	29.1 – 2.9	28.5 – 2.0
Total reflections used	14,452	25,848
Protein atoms	5239	2618
Non-protein atoms	74	80
RMSD bond lengths (Å)	0.007	0.015
RMSD bond angles (°)	1.0	1.5
R_{work}[d]	23.9 (35.1)[e]	20.7 (24.4)[e]
R_{free}[f]	29.6 (44.3)	25.2 (29.4)

[a]Diffraction from this crystal form was anisotropic, with maxima extending beyond 2.9 Å in the *b** direction, and from 3.5–4.5Å in orthogonal directions.

[b]$R_{sym} = \sum_h \sum_i |I(h)_i - I(h)| / \sum_h \sum_i I(h)_i$, where I(h) is the mean intensity of *i* reflections after rejections. A −0.5 I/σ_I cutoff was applied to the G$\alpha_{i/12}$ data set due to its anisotropic data.

[c]Numbers in parentheses correspond to the highest resolution shell of data for each set, which was 3.0 – 2.9 Å for G$\alpha_{i/12}$ and 2.07 – 2.00 Å for G$\alpha_{i/13}$.

[d]$R_{work} = \sum_{hkl} ||F_{obs}(hkl)| - |F_{calc}(hkl)|| / \sum_{hkl} |F_{obs}(hkl)|$; no I/σ cutoff was used during refinement.

[e]Numbers in parentheses correspond to the highest resolution shell of data for each set, which was 3.0 – 2.9 Å for G$\alpha_{i/12}$ and 2.05 – 2.00 Å for G$\alpha_{i/13}$.

[f]5% of the truncated data set was excluded from refinement to calculate R_{free}.